HHS Public Access

Author manuscript

Stem Cells. Author manuscript; available in PMC 2015 August 24.

Published in final edited form as:

Stem Cells. 2012 February ; 30(2): 253–265. doi:10.1002/stem.777.

Barx2 is Expressed in Satellite Cells and is Required for Normal Muscle Growth and Regeneration

Robyn Meech[a], **Katie N. Gonzalez**[b], **Marietta Barro**[c], **Anastasia Gromova**[c,d], **Lizhe Zhuang**[a], **Julie-Ann Hulin**[a], and **Helen P. Makarenkova**[c,d]

[a]Department of Clinical Pharmacology, Flinders University, Bedford Park, South Australia, Australia

[b]Molecular Diagnostic Services, Inc., San Diego, California, USA

[c]Department of Neurobiology, The Scripps Research Institute, La Jolla, California, USA

[d]The Neurosciences Institute, San Diego, California, USA

Abstract

Muscle growth and regeneration are regulated through a series of spatiotemporally dependent signaling and transcriptional cascades. Although the transcriptional program controlling myogenesis has been extensively investigated, the full repertoire of transcriptional regulators involved in this process is far from defined. Various homeodomain transcription factors have been shown to play important roles in both muscle development and muscle satellite cell-dependent repair. Here, we show that the homeodomain factor Barx2 is a new marker for embryonic and adult myoblasts and is required for normal postnatal muscle growth and repair. Barx2 is coexpressed with Pax7, which is the canonical marker of satellite cells, and is upregulated in satellite cells after muscle injury. Mice lacking the *Barx2* gene show reduced postnatal muscle growth, muscle atrophy, and defective muscle repair. Moreover, loss of *Barx2* delays the expression of genes that control proliferation and differentiation in regenerating muscle. Consistent with the in vivo observations, satellite cell-derived myoblasts cultured from *Barx2*$^{-/-}$ mice show decreased proliferation and ability to differentiate relative to those from wild-type or *Barx2*$^{+/-}$ mice. *Barx2*$^{-/-}$ myoblasts show reduced expression of the differentiation-associated factor myogenin as well as cell adhesion and matrix molecules. Finally, we find that mice lacking both *Barx2* and *dystrophin* gene expression have severe early onset myopathy. Together, these data indicate that Barx2 is an important regulator of muscle growth and repair that acts via the control of satellite cell proliferation and differentiation.

Correspondence: Helen P. Makarenkova, Ph.D., Department of Neurobiology, The Scripps Research Institute, 10550 North Torrey Pines Road, La Jolla, Califonia 92037, USA. Telephone: 858-784-2621; Fax: 858-784-2646; hmakarenk@scripps.edu.

Disclosure of Potential Conflicts of Interests

The authors indicate no potential conflicts of interests.

Author contributions: R.M.: conception and design, collection and/or assembly of data, data analysis and interpretation, manuscript writing, and final approval of manuscript; K.G., M.B.,A.G.,J.Z., and J.-A.H.: collection and/or assembly of data; H.M.: conception and design, financial support, collection and/or assembly of data, data analysis and interpretation, manuscript writing, and final approval of manuscript.

Keywords

Muscle stem cells; Adult stem cells; Homeobox genes; Muscular dystrophy; Skeletal muscle; Cell adhesion molecules; Tissue regeneration; Tissue-specific stem cells

Introduction

Adult mammalian muscle has the potential to regenerate by activation of undifferentiated myogenic precursor cells called satellite cells, which are normally quiescent and situated between the basal lamina and the myofiber plasmalemma [1–6]. On activation, satellite cells proliferate and divide asymmetrically producing one daughter cell that proceeds to myogenic differentiation and another that becomes quiescent and replenishes the satellite-cell pool [7, 8].

Satellite cells are estimated to account for approximately 30% of the nuclei in mouse limb muscle at birth; however, this pool diminishes as the cells are recruited for postnatal muscle growth [9]. In adults, substantial muscle growth ceases and the satellite cells, which account for less than 5% of the myonuclei, become quiescent until injury or exercise causes them to reenter the cell cycle [2]. Recent work shows that satellite cells are indispensable for adult skeletal muscle regeneration and cannot be compensated by other endogenous progenitor cells [10].

Several types of transcription factors control the specification, activation, proliferation, and differentiation of satellite cells, most prominently, members of the basic helix loop helix (bHLH) family and the paired and homeodomain families. Four bHLH myogenic regulatory factors (MRFs) act in a hierarchical fashion to orchestrate an embryonic muscle developmental program that involves myoblast determination, proliferation, migration, and differentiation [11–16]. The MRFs are also involved in various events downstream of satellite-cell activation during postnatal muscle growth and repair [17–19]. Homeobox transcription factors are key regulators of morphogenetic programs via activities such as the control of cell–cell and cell–substrate adhesion. Adhesion and signaling in turn influences cell activation, migration, and fusion [20]. Homeobox proteins play particularly important roles in embryonic and adult myogenesis. The best-characterized homeobox proteins in muscle development are the paired-homeodomain factors Pax3 and Pax7, which control the specification and migration of embryonic muscle precursors [21–23]. Pax7 is also expressed in all adult satellite cells, and Pax3 is present in a subset of muscle progenitor cells [24, 25]. Both Pax3 and Pax7 are involved in maintaining the myogenic identity of these cells and regulate entry into the myogenic program by activation of MyoD [25–27]. Pax7 is often considered the canonical marker for satellite cells and may promote satellite-cell survival and self-renewal [28, 29]. Other homeobox families involved in embryonic myogenesis include Pitx [30–32], Msx [33], Meox [34, 35], and Lbx [36, 37]. Some of these factors are also expressed in adult satellite cells where they may influence proliferation or differentiation [36, 38–40]. In general, however, the roles of non-paired homeodomain proteins in adult myogenesis are less well understood than in embryonic development.

In previous work, we showed that the antennapedia class Barx2 homeobox protein is a novel regulator of myogenesis. Barx2 interacts directly with MyoD and serum response factor (SRF) to regulate remodeling of the actin cytoskeleton and promote myoblast migration and differentiation in vitro [41, 42]. Barx2 also affects the morphological plasticity of nascent myofibres and controls expression of the cell-cycle factor cyclin-D1 [43]. Other known targets of Barx2 include genes involved in cell and substrate adhesion such as the neural cell adhesion molecule [44] and cadherins [45]. Moreover, the *Barx2* gene promoter is activated by MyoD and myogenin suggesting that it may be subject to muscle-specific regulatory feedback [46].

Here, we report that Barx2 is coexpressed with Pax7 in muscle progenitor cells during embryonic and fetal development and in the satellite cells of postnatal and adult muscles. Mice lacking the *Barx2* gene show reduced postnatal muscle growth, increased age-associated muscle atrophy, and impaired regeneration. Activation of genes involved in proliferation and differentiation are delayed after injury in *Barx2*$^{-/-}$ mice; this effect is recapitulated in cultured *Barx2*$^{-/-}$ myoblasts suggesting intrinsic impairment of myoblast function. Moreover, interbreeding of *Barx2* null mice with dystrophic *mdx* mice leads to a striking exacerbation of the disease phenotype. Overall, our data indicate that Barx2 is a new marker of satellite cells and myoblasts and is an important regulator of muscle growth, maintenance, and regeneration.

Materials and Methods

Mice

Barx2 null mice were obtained from Dr. Geoff Rosenfeld, maintained by heterozygous crosses and genotyped according to [47]. C57BL/10ScSn-Dmd^{mdx}/J (*mdx*) mice were obtained from Jackson Laboratories and interbred with *Barx2* null mice. See supporting information Methods for more details. All animal studies were approved by The Scripps Research Institute and Flinders University animal welfare committees.

Histology and Myofibre Diameter Analysis

Various dissected muscles were fixed with 4% paraformaldehyde (PFA) in PBT (phosphate buffered saline supplemented with 0.05% Tween 20) and processed for paraffin embedding. Muscle sections (10 μm) were processed for hematoxylin and eosin (H&E), Masson's Trichrome (to detect collagen deposition), and alizarin red (to detect calcification) staining at the Scripps Research Institute Histology core facility. To ensure that similar regions of muscle were compared between individuals, serial sections were cut from the midpoint of each fixed muscle specimen. Sections were examined using a Zeiss microscope. The maximal diameters of myofibers were measured in transverse sections from three different animals per genotype; approximately 400 myofibers were counted for each genotype. Myofiber diameters in micrometers were approximated using the scale bars on the micrographs.

Immunohistochemistry, Fluorescence Microscopy, and Image Analysis

Embryonic limbs and postnatal and adult muscles were fixed in 4% paraformaldehyde (PFA) washed in phosphate buffered saline (PBS) and frozen sections were prepared [48]. Sections were stained on slides with different combinations of primary antibodies: rabbit polyclonal anti-Barx2 (M-186, Santa Cruz Biotechnologies, Santa Cruz, CA, www.scbt.com), mouse monoclonal anti-skeletal myosin (Fast; clone MY-32, Sigma, St. Louis, http://www.sigmaaldrich.com), mouse monoclonal anti-MyoD, (clone MoAb5.8A, BD PharMingen, San Diego, CA, http://www.bdbiosciences.com/reagents/), mouse monoclonal anti-Myogenin (clone F5D BD Bioscience Pharmingen, San Diego, CA, http://www.bdbiosciences.com/reagents/), mouse monoclonal anti-Pax7 (R&D Systems, Minneapolis, MN, http://www.rndsystems.com/), goat polyclonal anti-Pax3 (Santa Cruz Biotechnologies, Santa Cruz, CA, www.scbt.com), rat anti-heparan sulfate (HS) proteoglycan monoclonal antibody (clone A7L6, Millipore, Billerica, MA, http://www.millipore.com/), mouse monoclonal anti-light meromyosin (clone MF20, Developmental Studies Hybridoma Bank, Iowa City, IA, http://dshb.biology.uiowa.edu/), and rabbit polyclonal Collagen I antibody (ab292) (Abcam). Fluorescent secondary antibodies for frozen sections were from Invitrogen (Molecular Probes, Grand Island, NY, http://www.invitrogen.com): Alexa Fluor-488 goat anti-mouse IgG1 (A21121), Alexa Fluor-633 goat anti-rat IgG (H+L) (A21094), Alexa Fluor-488 donkey anti-goat IgG (H+L) (A11055), Alexa Fluor-488 goat anti-mouse IgG (H+L) “highly cross-adsorbed” (A11029), Alexa Fluor-594 donkey anti-rabbit IgG (H+L) (A21207). For collagen staining on paraffin sections, we used horseradish peroxidise (HRP)-conjugated goat polyclonal secondary antibody to rabbit IgG (ab6721) (Abcam, Cambridge, UK, www.abcam.com), and the HRP reaction product was visualized using diaminobenzidine and counterstained with iron hematoxylin.

Single optical sections and Z-series were obtained using a Bio-Rad (Zeiss, Thornwood, NY, www.zeiss.com) Radiance 2100 Rainbow LSCM. The creation of three-dimensional images and animations using IMARIS software as well as calculation of colocalization are provided in the supporting information Methods [49].

Cardiotoxin Injection and Muscle Regeneration Analysis

Tibialis anterior (TA) muscles of anesthetized adult mice were injected with cardiotoxin or saline as described previously [50]. A detailed procedure is given in supporting information Methods. At various time points postinjection, muscles were harvested and either fixed with buffered 4% paraformaldehyde or processed in RNAlater (Ambion, Grand Island, NY, http://www.invitrogen.com) for preparation of RNA and gene expression analysis. Paraffin or frozen sections were prepared for H&E or antibody staining as described above. For gene expression analysis, *n* indicates the number of animals of each genotype, and the significance of the result was assessed using a Student’s *t* test.

Preparation of Primary Myoblasts, Imaging, and Proliferation Analysis

Primary myoblast cultures were prepared using all muscles from the hind limbs of four to five pups (pooled and minced together) as described previously [51]. *Barx2*$^{-/-}$ and *Barx2*$^{+/+}$ or *Barx2*$^{+/-}$ pups were age-matched (sibs or inbred cousins), and cultures were generated

simultaneously using identical conditions. Cells were grown on plates or chamber slides coated with 50 μg/ml collagen type I and maintained in growth medium (1:1 Ham's F10/ Dulbecco's modified Eagle's medium [DMEM], supplemented with 20% fetal bovine serum (FBS) and 2.5 ng/ml of basic fibroblast growth factor (bFGF)). Differentiation medium was DMEM supplemented with 2% horse serum. Proliferation was assessed on cells grown on chamber slides using the Cell Proliferation Kit (Amersham, Scientifics) with antibodies to Bromodeoxyuridine (BrdU) followed by Alexa-conjugated secondary antibodies (Invitrogen) and imaging under a Leica MZ FLIII fluorescence microscope. At least five randomly selected fields were analyzed on each of several replicate slides to determine the average percentage of cells incorporating BrdU. Significance was assessed using the nonparametric Wilcoxon signed-rank test. Proliferation and morphology data are shown from one set of matched myoblast cultures (*n* indicates the total number of fields counted across several slides); however, similar results were seen in replicate myoblast isolates.

RNA and Reverse-Transcriptase Polymerase Chain Reaction (RT-PCR)

RNA was prepared from cell cultures and from muscle tissue using Trizol reagent (Gibco, Grand Island, NY, www.invitrogen.com). Cells were lysed directly in Trizol; muscle was ground with a pestle. RNA was DNAse-treated and reverse transcribed using random primers and MMluV reverse transcriptase (New England Biolabs, Ipswich, MA, www.neb.com). Quantitative RT-PCR reactions were performed on a Corbett Rotogene machine (Qiagen, Valencia, CA, www.qiagen.com) using GoTaq SYBR green reagents (Promega, Madison, WI, www.promega.com). Data were analyzed using the ΔΔCt method with comparison to a pool of housekeeping genes (18S ribosomal RNA, ribosomal protein S26, and glyceraldehyde-3-phosphate dehydrogenase [GAPDH]). Primer sequences are provided in the supporting information Methods.

Plate-Washing Assay

To assess the strength of cell adherence to a substrate, *Barx2*$^{+/-}$ and *Barx2*$^{-/-}$ primary myoblasts were cultured for 24 hours on 100-mm dishes that had been coated with 1 μg/ml fibronectin (Sigma, St. Louis, http://www.sigmaaldrich.com). Plates were then rinsed gently with PBS, covered with 7 ml of fresh PBS, and transferred to a slow-moving shaker for 15 min which allows weakly adherent cells to detach. The PBS was collected, centrifuged, and the detached cells were resuspended and counted. The experiment was repeated with three different myoblast isolates and all data were averaged. The significance of the results was assessed using the non-parametric paired test [52].

Results

Barx2 is Coexpressed with Pax7 in Embryonic and Adult Muscles

We previously showed that Barx2 is expressed in the ventral portion of embryonic limbs including putative early muscle masses [53]. To better understand the functions of Barx2 in muscle, we examined its expression pattern with respect to other muscle markers in embryonic, fetal, and adult mice.

Coimmunostaining of sections from E13.5 limbs with Barx2 and myosin heavy chain (MyHC) antibodies showed that Barx2 was expressed in a subset of nuclei within primary myofibers as well as in nuclei located between the fibers that are likely to represent undifferentiated myoblasts (Fig. 1A; Supporting Informtion Movie 1). Coimmunostaining with Barx2 and MyoD antibodies showed that these factors overlapped in many but not all nuclei (Fig. 1B, 1C). Pax7 is expressed in proliferating progenitors and differentiating myoblasts in embryonic and fetal muscle but is downregulated in myofibers [22, 54]. Coimmunostaining of fetal (E18) muscle with Barx2 and Pax7 antibodies revealed almost complete overlap in the expression of these two factors (Fig. 1D–1H), although Pax7-positive cells showed varying intensities of the Barx2 label (Fig. 1H, red arrowheads).

In adult muscle, Pax7 is a marker for quiescent satellite cells as well as activated, proliferating satellite cells during muscle regeneration [22, 55, 56]. Coimmunostaining with Barx2 and Pax7 antibodies revealed that essentially all Pax7-positive nuclei also expressed Barx2 (an example of coexpression is shown in Fig. 1I–1L, yellow arrow). There was also expression of Barx2 in a population of apparently Pax7-negative cells that remain to be further characterized (Fig. 1I–1L, white arrows). To confirm the interpretation that the Barx2/Pax7-positive cells are satellite cells, we used an antibody to HS to mark the basal lamina. Essentially all Barx2/Pax7-positive cells were situated under the basal lamina (Fig. 1M–1P, yellow arrows). Thus the data indicate that Barx2 is a new marker for adult satellite cells.

Barx2 Knockout Mice Show Delayed Postnatal Muscle Growth and Adult Muscle Atrophy

To determine whether Barx2 is important for muscle development and growth, we examined the phenotype of embryonic and postnatal *Barx2*$^{-/-}$ mice. There were no obvious differences in body size, or muscle size, or morphology between wild-type, *Barx2*$^{+/-}$, and *Barx2*$^{-/-}$ embryos at E12.5–18.0 (not shown) and no difference in body weight at birth (Fig. 2A). However, by postnatal day 4, *Barx2*$^{-/-}$ mice showed a 10% reduction in body weight relative to *Barx2*$^{-/+}$ and *Barx2*$^{+/+}$ littermates (Fig. 2A) indicating a growth delay. The delay became most pronounced at approximately 4 weeks of age when *Barx2*$^{-/-}$ mice were typically 20–25% smaller than their *Barx2*$^{-/+}$ and wild-type littermates (Fig. 2A, 2B). The size difference was independent of sex. There was no overt sign of feeding difficulties in *Barx2*$^{-/-}$ mice relative to wild-type or heterozygous littermates and the stomachs of pups were full of milk. Older *Barx2*$^{-/-}$ mice (15–18 months) often showed musculoskeletal abnormalities such as spinal curvature, splayed stance, and “waddling” gait that were not apparent in wild-type or heterozygous mice at this age (Fig. 2E, supporting information Fig. 1 and supporting information Movies 2, 3).

The masses of individual limb muscles were found to be reduced in adult *Barx2*$^{-/-}$ mice relative to *Barx2*$^{+/-}$ or wild-type mice. TA and quadriceps muscles from 4-week-old *Barx2*$^{-/-}$ mice weighed 20%–30% less than those of their *Barx2*$^{+/-}$ littermates (Fig. 2C), while the soleus muscle was reduced by almost 60% in *Barx2*$^{-/-}$ mice (Fig. 2C, 2D). The muscles were reduced in disproportion to overall body mass and the mass of other organs (Fig. 2C). Measurements of myofiber diameters in transverse sections of adult soleus muscles demonstrated a change in myofibre size distribution: *Barx2*$^{-/-}$ muscles contained

fewer large fibers and a greater number of smaller myofibres relative to *Barx2*$^{+/+}$ (Fig. 2F) or *Barx2*$^{+/-}$ (not shown) muscles. RT-PCR analysis revealed approximately 60% reduction in myogenin mRNA levels in adult *Barx2*$^{-/-}$ muscles relative to *Barx2*$^{+/-}$ muscles. (Fig. 2G).

Histological analysis of *Barx2*$^{-/-}$ and wild-type muscles at 6 and 12 months of age revealed striking differences in muscle appearance. TA, soleus, and diaphragm muscles from *Barx2*$^{+/+}$ and *Barx2*-littermates were examined by H&E staining of paraffin-embedded serial sections. For each group, four to five mice were analyzed and representative images of 6-month-old mice are shown in Figure 3. Transverse sections of the *Barx2*$^{-/-}$ TA revealed narrower myofibers and greater variability in myofiber size and shape relative to the wild-type muscle (compare Fig. 3A, 3B and 3D, 3E). Masson's trichrome staining for collagen expression revealed endomysial and perimysial collagen deposition suggesting fibrosis in *Barx2*$^{-/-}$ TA muscle (Fig. 3C, 3F).

Barx2$^{-/-}$ soleus muscles exhibited narrower myofibers (Fig. 2F), more rounded myofibers, and an increased distance between myofibers compared to the soleus muscles of wild-type mice (Fig. 3G–3I). Variation in interstitial space may be due to changes in osmotic pressure during dissection, although sections of *Barx2*$^{-/-}$ soleus also showed increased staining with collagen I antibodies suggesting perimysial fibrosis (Fig. 3J–3L). We also found groups of angulated atrophic fibers (Fig. 3I, black arrowheads). Diaphragm muscle was also dramatically affected by loss of Barx2; diaphragms of 6-month-old *Barx2*$^{-/-}$ mice were substantially thinner than those of wild-type littermates (Fig. 3M–3R) and this was largely associated with thinner myofibers. There was only mild fibrosis of the diaphragm muscle at this age (Fig. 3O, 3R). Comparison of 6- and 12-month-old *Barx2*$^{-/-}$ muscle sections suggested that the muscle defects worsened as animals became older (not shown).

Barx2 Is an Important Regulator of Muscle Regeneration

To determine whether Barx2 expression is involved in regeneration after acute muscle injury, we performed intramuscular injection of cardiotoxin [50] in *Barx2*$^{+/-}$ mice and examined Barx2 expression by immunostaining. On day 4 after injection, the number of Barx2-expressing cells increased dramatically in the cardiotoxin-injected TA muscle but not in the control, saline-injected muscle (Fig. 4A, 4B). RT-PCR analysis of the injected muscles confirmed increased Barx2 mRNA expression 4 days after injury (Fig. 4C). Most cells that expressed Barx2 in regenerating muscle also expressed Pax7, suggesting that these are activated and proliferating satellite cells (Fig. 4D).

Barx2$^{+/+}$, *Barx2*$^{+/-}$, and *Barx2*$^{-/-}$ TA muscles were examined histologically 10 days after cardiotoxin injury. *Barx2*$^{+/+}$ (Fig. 4E) and *Barx2*$^{+/-}$ (not shown) muscle showed efficient regeneration as indicated by many new myofibers with centrally located nuclei. In contrast, in *Barx2*$^{-/-}$ muscle, necrosis was still evident; there were more mononucleate cells, and regenerating myofibers were more irregular in shape and size than in *Barx2*$^{+/-}$ muscle (Fig. 4F). Alizarin red staining, which identifies fibers with high intracellular calcium in dystrophic muscles [57], revealed frequent calcium deposits in the regenerating muscles of *Barx2*$^{-/-}$ but not *Barx2*$^{+/-}$ mice (Fig. 4E, 4F insets).

We next examined whether loss of *Barx2* altered the normal temporal pattern of gene expression during muscle repair. The TA muscles of *Barx2*$^{-/-}$ or control (*Barx2*$^{+/+}$ and Barx2$^{+/-}$) mice were injected with cardiotoxin or saline (in the contralateral limb); muscles were harvested at 2, 5, and 12 days after injury for isolation of RNA. At day 2 after injection, the expression of cyclin-D1 was induced nearly 14-fold in cardiotoxin-treated muscle relative to saline-treated muscle in *Barx2*$^{+/+}$ and *Barx2*$^{+/-}$ mice (controls). In contrast, *Barx2*$^{-/-}$ mice showed less than fourfold induction of cyclin-D1 at this time. The difference in cyclin-D1 expression between genotypes was no longer significant at day 5 (Fig. 4G). Myogenin showed nearly threefold induction by day 2 after cardiotoxin treatment in control mice suggesting that differentiation begins while myoblast proliferation is ongoing. This is in agreement with previous studies [58]. In contrast, there was no induction of myogenin at day 2 in *Barx2*$^{-/-}$ mice (Fig. 4H). Myogenin expression was induced nearly 40-fold at day 5 in control mice, and while apparently lower in *Barx2*$^{-/-}$ mice this was not statistically significant (Fig. 4H). By day 12 after treatment, myogenin expression was reduced to baseline in controls suggesting that the differentiation phase is complete. However, myogenin expression remained significantly elevated in *Barx2*$^{-/-}$ mice at this time. This pattern suggests a temporal shift in myogenin expression after injury and is similar to that reported previously for mice lacking the Mnf1 forkhead factor [58]. Finally, expression of MyHC 4 (Myh4), which is a marker for myofibers, is lower in *Barx2*$^{-/-}$ mice than control mice at day 12 after injury (Fig. 4I). This is consistent with the appearance of fewer regenerated myofibers in *Barx2*$^{-/-}$ muscle sections (Fig. 4F).

Barx2$^{-/-}$ Myoblasts Show Altered Morphology and Reduced Proliferation in Culture

We prepared cultures of satellite-cell derived myoblasts from postnatal day 4 (P4) muscles [51]; these cultures contain primarily proliferating myoblasts expressing Pax7 and MyoD. In line with previous report [59], we found that cultured myoblasts displayed two different morphologies: rounded cells with smooth membranes (Fig. 5A, black arrows) and more elongated and flattened cells with processes (Fig. 5A, red arrows). The “rounded” and “flattened” myoblasts were examined in more detail by confocal imaging after staining with antibodies to smooth muscle actin (SMA), which is expressed transiently in undifferentiated myoblasts [41, 60]. The flattened morphology was associated with cell spreading, filamentous actin redistribution, and increased numbers of cell surface protrusions (Fig. 5B–5D). Both rounded and flattened cells expressed Pax7 (not shown), consistent with undifferentiated myoblasts.

When we compared cultures derived from *Barx2*$^{-/-}$ muscle with cultures derived from *Barx2*$^{+/-}$ (Fig. 5E) or wild-type (not shown) muscle, we found that *Barx2*$^{-/-}$ cells were more likely to be rounded. Specifically, only 20% of cells showed the flattened morphology in *Barx2*$^{-/-}$ cultures whereas greater than 60% of cells had this morphology in *Barx2*$^{+/-}$ cultures (Fig. 5E). This suggests that absence of Barx2 results in decreased spreading and thus a reduced area of cell/substrate interaction. This result is in agreement with our previous findings that Barx2 regulates SMA expression, cell adhesion, and cell migration [41, 53, 61].

It has been previously reported that rounded myoblasts proliferate more slowly than flattened myoblasts in culture [59]. Consistent with this, analysis of BrdU incorporation showed that *Barx2*$^{-/-}$ myoblast cultures had decreased proliferation relative to *Barx2*$^{+/-}$ cultures (Fig. 5F).

Barx2$^{-/-}$ Myoblasts Show Delayed Differentiation and *Barx2*$^{-/-}$ Myotubes Have Poor Substrate Adhesion

On serum withdrawal, myoblasts in culture cease to divide and begin to express differentiation markers [41, 62]. It has been reported that rounded myoblasts are less differentiation-competent than flattened myoblasts [59]. We examined the expression of the differentiation markers myogenin and heavy chain myosin in *Barx2*$^{-/-}$ and *Barx2*$^{+/-}$ myoblast cultures after serum withdrawal. After 6 hours of serum withdrawal, *Barx2*$^{-/-}$ cultures contained fewer myogenin-expressing cells than *Barx2*$^{+/-}$ cultures (Fig. 6A, 6B) and at 24 hours *Barx2*$^{-/-}$ cultures contained fewer fast MyHC-expressing myotubes (Fig. 6C, 6D). Thus loss of Barx2 expression impairs the response of myoblasts to terminal differentiation signals and delays morphological differentiation.

Although *Barx2*$^{-/-}$ myoblasts were delayed in differentiation over the first 24 hours after serum withdrawal, by 48 hours most of *Barx2*$^{-/-}$ myoblasts had formed short myotubes. However, between 48 and 72 hours many nascent *Barx2*$^{-/-}$ myotubes assumed an irregular curve shape in contrast to the uniformly straight elongated *Barx2*$^{+/-}$ myotubes (Fig. 6E). The irregular shape appeared to be due to partial detachment of the myotubes from the collagen substrate.

To determine whether *Barx2*$^{-/-}$ and *Barx2*$^{+/-}$ myoblasts have reduced adhesion properties, we seeded *Barx2*$^{+/-}$ and *Barx2*$^{-/-}$ myoblasts onto dishes coated with fibronectin instead of collagen. Our experience with wild-type myoblasts indicated that fibronectin mediates only weak attachment of myoblasts and delays myotube formation by several days relative to collagen. It has also been recently reported by others that myoblasts plated on fibronectin adhere weakly [63]. Cells were grown for 48 hours and then transferred to differentiation medium for 7–8 days. *Barx2*$^{+/-}$ cells formed myotubes after 1 week whereas *Barx2*$^{-/-}$ myoblasts failed to form myotubes and remained rounded and poorly attached (Fig. 6G). We also performed a plate-washing assay to determine how readily myoblasts detached from the fibronectin coated plate. Plates were rinsed five times with PBS, the rinsates were combined, and the numbers of cells that they contained were counted. Nearly three times more *Barx2*$^{-/-}$ cells were detached from the plates than *Barx2*$^{+/-}$ cells (Fig. 6F), indicating that their adhesion to a fibronectin substrate is substantially reduced.

To better understand the mechanism of reduced substrate adhesion in *Barx2*$^{-/-}$ myoblast cultures, we examined gene expression profiles of cultured wild-type and *Barx2*$^{-/-}$ myoblasts using a PCR array focused on extracellular matrix and adhesion molecule genes (SABiosciences). A total of 15 genes involved in regulation of cell adhesion and cell matrix remodeling showed greater than twofold decrease in expression in *Barx2*$^{-/-}$ myoblasts relative to wild-type myoblasts (supporting information Table 1). This result correlates with our previous findings that Barx2 is involved in regulation of cell adhesion in mesenchymal progenitor cells [44, 46, 53] and that ectopic Barx2 expression could induce matrix

metalloprotease (MMP) expression in MCF7 cells [61]. Downregulation of cell adhesion and matrix remodeling molecules in *Barx2*$^{-/-}$ myoblasts could contribute to impaired substrate attachment, migration, and fusion [41], thus delaying differentiation.

Loss of *Barx2* Exacerbates the Dystrophic Phenotype in *mdx* Mice

To better understand the role of Barx2 in muscle repair, we examined the effects of *Barx2* deletion in the *mdx* mouse model of human Duchenne muscular dystrophy (DMD) and Becker muscular dystrophy [64]. *Mdx* mice carry a loss-of-function point mutation in the X-linked *dystrophin* gene. Although *mdx* mice display extensive necrosis of muscle fibers at 2 weeks of age, they maintain muscle integrity due to a high regenerative capacity, which leads to hypertrophy [65–67]. Except in the diaphragm, adult *mdx* mice do not display the muscle fiber loss and extensive interstitial fibrosis observed in human DMD patients. Moreover, *mdx* mice display normal external appearance and only moderately reduced life spans [68].

We crossed Barx2 mutant and *mdx* mice and inbred the "*Barx2:mdx*" double mutants for up to nine generations to reduce genetic variability. By six generations, crosses between mice that were both heterozygous for *Barx2* and null for *dystrophin* (i.e., *Barx2*$^{+/-}$*:mdx*) produced litters in which *Barx2*$^{-/-}$*:mdx* mice were significantly under-represented by weaning age (supporting information Table 2). This was in contrast to *Barx2*$^{-/-}$ mice on the C57Bl/6 background that retained normal mendelian ratios. It is notable that *MyoD*$^{-/-}$*:mdx* double mutant mice become nonviable around the ninth generation [69]. Our subsequent analyses were performed on eighth to tenth generation mice.

Barx2$^{+/+}$*:mdx* and *Barx2*$^{-/-}$*:mdx* sibling pairs (all of which were null for dystrophin) were collected and body, muscle, and organ weights were measured. *Barx2*$^{-/-}$*:mdx* were at approximately 30% smaller than *Barx2*$^{+/+}$*:mdx* mice at 4 weeks of age and organs such as kidney were reduced proportionately (~ 30%), However, the TA muscle in *Barx2*$^{-/-}$*:mdx* mice weighed on average 50% less than that in *Barx2*$^{+/+}$*:mdx* mice (Fig. 7A). suggesting that muscle is specifically wasted in *Barx2*$^{-/-}$*:mdx* mice (Fig. 7A). This reduction in TA weight is also more dramatic than that observed in *Barx2*$^{-/-}$ mice that have a functional dystrophin gene (Fig. 2).

Barx2$^{-/-}$*:mdx* mice also developed spine deformation resembling kyphosis by 6 months of age and became progressively weak and less ambulatory with a waddling gait. Although similar characteristics were observed in some older *Barx2*$^{-/-}$ mice (Fig. 2), this pathology appeared earlier and with greater penetrance in *Barx2*$^{-/-}$*:mdx* mice.

Sections of TA muscles from 6-month-old *Barx2*$^{-/-}$, *Barx2*$^{+/+}$*:mdx* and *Barx2*$^{-/-}$*:mdx* mice were examined histologically and compared to those from *Barx2*$^{-/-}$ mice (Fig. 7B–7D). *Barx2*$^{+/+}$*:mdx* muscle showed variability in myofiber size as well as many central nuclei indicating ongoing repair of muscle damage as would be expected in *mdx* muscle at this age (Fig. 7C). In contrast, the organization of *Barx2*$^{-/-}$*:mdx* TA muscle appeared extremely aberrant with greater variability in myofiber size and fewer central nuclei relative to muscle from *Barx2*$^{+/+}$*:mdx* mice suggesting less repair (Fig. 7D). *Barx2*$^{-/-}$*:mdx* soleus muscles also

showed greater variability in myofiber size and shape as well as more endomysial and perimysial fibrosis relative to the soleus muscles of *Barx2*$^{+/+}$*:mdx* mice (Fig. 7F–7L).

The diaphragm muscles (Fig. 7Q) of 6-month-old *Barx*$^{-/-}$*:mdx* mice appeared much thinner than the diaphragms of *Barx2*$^{+/+}$*:mdx* mice (Fig. 7N). In addition, diaphragms of *Barx2*$^{-/-}$*:mdx* mice showed more frequent rounded opaque fibers (dark red and glassy, black arrows) often with clear vacuoles (compare Fig. 7M and 7O). These are hypercontracted atrophic fibers. At 12 months, diaphragms of *Barx2*$^{-/-}$*:mdx* mice show a greater instance of focal myofiber necrosis and necrotic myofibers undergoing myophagocytosis (compare Fig. 7P and 7T) as well as much more fibrosis (compare Fig. 7S and 7U), relative to *Barx2*$^{+/+}$*:mdx* mice. Alizarin red staining revealed greatly increased calcium deposits in *Barx2*$^{-/-}$*:mdx* diaphragm muscles relative to *Barx2*$^{+/+}$*:mdx* mice (compare Fig. 7V, 7W and 7X, 7Y). While some of the histological features of *Barx2*$^{-/-}$*:mdx* muscles were also observed in *Barx2*$^{-/-}$ muscles (Fig. 3), the latter do not show the degenerative character of the *mdx* model, and fibrosis and calcium deposition is less pronounced.

Discussion

Our studies identify Barx2 as an important new regulator of myogenesis that is expressed in embryonic myoblasts as well as adult satellite cells and is required for normal muscle growth, maintenance, and regeneration.

Overlapping Functions for Barx2 and Pax7 in Muscle Progenitor Cells

Barx2 is expressed in muscle progenitor cells at embryonic, juvenile, and adult stages in a pattern that overlaps extensively with Pax7 expression, suggesting that Barx2 is a new marker for embryonic and fetal myoblasts and adult satellite cells. We also observed a population of Barx2-positive/Pax7-negative mononucleate cells in adult muscle suggesting that in addition to satellite cells, Barx2 is expressed in some interstitial cells or another muscle progenitor type [70–73]. Studies of Barx2-expressing cell populations in muscle are ongoing.

The *Barx2* null mouse shows several parallels with the *Pax7* germline null model. Embryonic muscle development in *Pax7* germline null mice is grossly normal [74]; however, postnatal muscle growth and regeneration in these mice is severely impaired [28, 74, 75]. Similarly, *Barx2* null mice show apparently normal embryonic development but moderately impaired postnatal muscle growth and maintenance, and severely impaired regeneration. We observed no alteration of the Pax7 expression pattern in *Barx2* null mice by immunostaining (not shown), although Pax7 expression was slightly reduced in *Barx2* null muscle by RT-PCR and in cultured *Barx2* null myoblasts (supporting information Fig. 2). Currently, it is unclear whether this has any role in the phenotype of *Barx2* null mice; Barx2 and Pax7 may function in parallel pathways. It was recently shown that conditional *Pax7* null mice in which *Pax7* is deleted after 4 weeks of age have no defects in muscle maintenance or regeneration after acute injury [76]. This suggests compensation by other factors potentially working in parallel with Pax7 in adult muscle; Barx2 might be one such factor.

Barx2 Regulates the Proliferation and Differentiation of Satellite Cells in Culture

A previous study described populations of satellite cell-derived myoblasts with “round” and “thick” morphologies that grow clonally on isolated myofibers [59]. The round cells were shown to be directly descended from satellite cells and were described as having “stem cell-like characteristics” being slow-dividing and self-renewing. The thick cells were the rapidly dividing, differentiation competent progeny of the round cells [59]. Our satellite cell-derived myoblast cultures (from mice of all genotypes) contained “rounded and flattened cells” that appeared to correspond to the “round and thick” morphologies described by Hashimoto et al. [59]. However, *Barx2*$^{-/-}$ myoblasts showed a predominantly rounded morphology in culture and consistent with this, they were less proliferative and markedly delayed in differentiation when compared to wild-type or heterozygous cells. These data indicate that myoblasts lacking *Barx2* tend to retain a primitive state marked by a reduced capacity for proliferation and differentiation.

The presence of fewer flattened cells in *Barx2*$^{-/-}$ cultures also suggests defects in cell spreading and is consistent with our previous observations that *Barx2*$^{-/-}$ primary myoblasts show delayed cytoskeletal remodeling and SMA upregulation after serum withdrawal [41]. This SMA-associated remodeling is an important early step in myoblast differentiation that facilitates the migration and alignment of myoblasts for fusion. Overall, the delay in fusion of *Barx2*$^{-/-}$ myoblasts in this study agrees with our previous data showing that Barx2 cooperates with MRFs and that its overexpression accelerates differentiation of C2C12 myoblasts [41, 46].

Nascent *Barx2*$^{-/-}$ myofibers showed reduced substrate adhesion leading to a curved shape and *Barx2*$^{-/-}$ myoblasts had reduced expression of cell adhesion and matrix molecules, including integrins and cell adhesion molecules (CAMs) that are known to be important for cell spreading and differentiation in culture [77–79]. Moreover, reduced expression of particular CAMs could compromise crosstalk between the satellite cell and the myofiber in vivo [80, 81]. Barx2 expression is downregulated in mature myofibers [43]. Presumably, therefore, the effect of *Barx2* gene deletion would be more acute in nascent than in mature myofibers. Consistent with this, we recently found that forcing a high level of Barx2 expression in young but not mature myofibers affects their morphological stability [43]. Overall, our data suggest that Barx2 facilitates the emergence of fast dividing, differentiation-competent myoblasts and promotes differentiation by altering the expression of both regulatory and mechanochemical factors.

The Role of Barx2 in Muscle Growth, Maintenance, and Regeneration

Satellite cells are required for postnatal muscle growth, are activated when the muscle is overloaded [82], and mediate repair of muscle injury [83]. Moreover, diseases involving accelerated muscle atrophy such as congenital myotonic dystrophy are suggested to involve impaired satellite cell function [84]. Based on our observations that Barx2 is predominantly expressed in satellite cells and their myoblast progeny and that lack of Barx2 delays myoblast proliferation and differentiation in vitro, it is most likely that delayed muscle growth in *Barx2*$^{-/-}$ pups, the atrophic phenotype of adult *Barx2*$^{-/-}$ muscle, and lack of repair after injury are due to satellite cell/myoblast dysfunction.

Regarding the precise nature of this dysfunction, our muscle injury studies show misregulation of cell cycle and myogenic genes in regenerating *Barx2* null muscle. Lower cyclin-D1 expression in *Barx2*$^{-/-}$ mice at day 2 after cardiotoxin injury is consistent with delay in satellite cell activation and/or reduced proliferation of their progeny myoblasts. Delayed upregulation of myogenin at day 2 and sustained expression of this gene at day 12, together with reduced expression of the myofibre marker Myh4 at day 12 in *Barx2*$^{-/-}$ mice, are consistent with delayed onset and progression of differentiation. While it remains to be determined whether these gene expression changes are a cause or consequence of impaired proliferation and differentiation, the observation that Barx2 overexpression [43] or loss of expression (this study) in myoblast culture also alters expression of these genes suggests that Barx2 may be a direct effector of their regulation.

Impaired satellite cell and myoblast function in the absence of Barx2 is also likely to underlie the phenotype of the *Barx2/mdx* mouse model. The muscle of homozygous *mdx* mice is characterized by ongoing degeneration and regeneration of myofibers leading eventually to accumulation of fibrous and fatty infiltrates [85]. However, muscle function is maintained in young *mdx* mice, likely because repair is able to keep pace with injury. In contrast, double mutant *Barx2−/−:mdx* mice display increased penetration of the disease with phenotypic similarity to human DMD. Even young *Barx2−/−:mdx* mice showed extremely aberrant repair and extensive fibrous infiltration and calcification, which are consistent with impaired satellite cell/myoblast function. The mice also display gross musculoskeletal abnormalities including changes in gait, the latter resembling the waddling gait of boys with DMD due to contracture of the Achilles tendons [86]. The rapid and severe decline in muscle integrity in *Barx2*$^{-/-}$*:mdx* mice suggests that they may be useful model for studies of DMD.

Conclusion

Based on our current studies and previous work [41, 46], we conclude that Barx2 is a key regulator of proliferation and differentiation competence in satellite cell-derived myoblasts; in the absence of the vital activities of Barx2, satellite cell-mediated muscle maintenance and regeneration is grossly impaired.

Supplementary Material

Refer to Web version on PubMed Central for supplementary material.

Acknowledgments

We thank Kathryn Crossin and Bruce Cunningham for critical reading of the manuscript. This work was supported by National Institutes of Health Grant 5R01AR053163 (to H.P.M. and R.M.) and by a grant from the Association Francaise contre les Myopathies (to H.P.M.). This study was also supported by the Neurosciences Support Foundation (to H.P.M).

References

1. Mauro A. Satellite cell of skeletal muscle fibers. J Cell Biol. 1961; 9:493–495.
2. Schultz E, Gibson MC, Champion T. Satellite cells are mitotically quiescent in mature mouse muscle: An EM and radioautographic study. J Exp Zool. 1978; 206:451–456. [PubMed: 712350]

3. Asakura A, Rudnicki MA, Komaki M. Muscle satellite cells are multi-potential stem cells that exhibit myogenic, osteogenic, and adipogenic differentiation. Differentiation. 2001; 68:245–253. [PubMed: 11776477]
4. Gargioli C, Slack JMW. Cell lineage tracing during *Xenopus* tail regeneration. Development. 2004; 131:2669–2679. [PubMed: 15148301]
5. Montarras D, Morgan J, Collins C, et al. Direct isolation of satellite cells for skeletal muscle regeneration. Science. 2005; 309:2064–2067. [PubMed: 16141372]
6. Meeson AP, Hawke TJ, Graham S, et al. Cellular and molecular regulation of skeletal muscle side population cells. Stem Cells. 2004; 22:1305–1320. [PubMed: 15579648]
7. Shinin V, Gayraud-Morel B, Gomès D, et al. Asymmetric division and cosegregation of template DNA strands in adult muscle satellite cells. Nat Cell Biol. 2006; 8:677–682. [PubMed: 16799552]
8. Kuang S, Kuroda K, Le Grand F, et al. Asymmetric self-renewal and commitment of satellite stem cells in muscle. Cell. 2007; 129:999–1010. [PubMed: 17540178]
9. Cardasis CA, Cooper GW. An analysis of nuclear numbers in individual muscle fibers during differentiation and growth: A satellite cell-muscle fiber growth unit. J Exp Zool. 1975; 191:347–358. [PubMed: 1127400]
10. Sambasivan R, Yao R, Kissenpfennig A, et al. Pax7-expressing satellite cells are indispensable for adult skeletal muscle regeneration. Development. 2011; 138:3647–3656. [PubMed: 21828093]
11. Rudnicki MA, Schnegelsberg PN, Stead RH, et al. MyoD or Myf-5 is required for the formation of skeletal muscle. Cell. 1993; 75:1351–1359. [PubMed: 8269513]
12. Tajbakhsh S, Bober E, Babinet C, et al. Gene targeting the myf-5 locus with nlacZ reveals expression of this myogenic factor in mature skeletal muscle fibres as well as early embryonic muscle. Dev Dyn. 1996; 206:291–300. [PubMed: 8896984]
13. Kassar-Duchossoy L, Gayraud-Morel B, Gomès D, et al. Mrf4 determines skeletal muscle identity in Myf5:Myod double-mutant mice. Nature. 2004; 431:466–471. [PubMed: 15386014]
14. Hinterberger TJ, Sassoon DA, Rhodes SJ, et al. Expression of the muscle regulatory factor MRF4 during somite and skeletal myofiber development. Dev Biol. 1991; 147:144–156. [PubMed: 1715299]
15. Brennan TJ, Edmondson DG, Olson EN. Aberrant regulation of MyoD1 contributes to the partially defective myogenic phenotype of BC3H1 cells. J Cell Biol. 1990; 110:929–937. [PubMed: 1691195]
16. Pownall ME, Gustafsson MK, Emerson CP. Myogenic regulatory factors and the specification of muscle progenitors in vertebrate embryos. Annu Rev Cell Dev Biol. 2002; 18:747–783. [PubMed: 12142270]
17. Fuchtbauer EM, Westphal H. MyoD and myogenin are coexpressed in regenerating skeletal muscle of the mouse. Dev Dyn. 1992; 193:34–39. [PubMed: 1311614]
18. Cooper RN, Tajbakhsh S, Mouly V, et al. In vivo satellite cell activation via Myf5 and MyoD in regenerating mouse skeletal muscle. J Cell Sci. 1999; 112:2895–2901. [PubMed: 10444384]
19. Charge SBP, Rudnicki MA. Cellular and molecular regulation of muscle regeneration. Physiol Rev. 2004; 84:209–238. [PubMed: 14715915]
20. Morgan BA, Tabin C. Hox genes and growth: Early and late roles in limb bud morphogenesis. Dev Suppl. 1994:181–186. [PubMed: 7579519]
21. Bober E, Franz T, Arnold HH, et al. Pax-3 is required for the development of limb muscles: A possible role for the migration of dermomyotomal muscle progenitor cells. Development. 1994; 120:603–612. [PubMed: 8162858]
22. Relaix F, Rocancourt D, Mansouri A, et al. A Pax3/Pax7-dependent population of skeletal muscle progenitor cells. Nature. 2005; 435:948–953. [PubMed: 15843801]
23. Kassar-Duchossoy L, Giacone E, Gayraud-Morel B, et al. Pax3/Pax7 mark a novel population of primitive myogenic cells during development. Genes Dev. 2005; 19:1426–1431. [PubMed: 15964993]
24. Kirkpatrick LJ, Yablonka-Reuveni Z, Rosser BW. Retention of Pax3 expression in satellite cells of muscle spindles. J Histochem Cytochem. 2010; 58:317–327. [PubMed: 20026670]

25. Buckingham M. Skeletal muscle progenitor cells and the role of Pax genes. C R Biol. 2007; 330:530–533. [PubMed: 17631448]
26. Relaix F, Montarras D, Zaffran S, et al. Pax3 and Pax7 have distinct and overlapping functions in adult muscle progenitor cells. J Cell Biol. 2006; 172:91–102. [PubMed: 16380438]
27. Zammit PS, Relaix F, Nagata Y, et al. Pax7 and myogenic progression in skeletal muscle satellite cells. J Cell Sci. 2006; 119:1824–1832. [PubMed: 16608873]
28. Oustanina S, Hause G, Braun T. Pax7 directs postnatal renewal and propagation of myogenic satellite cells but not their specification. EMBO J. 2004; 23:3430–3439. [PubMed: 15282552]
29. McFarlane C, Hennebry A, Thomas M, et al. Myostatin signals through Pax7 to regulate satellite cell self-renewal. Exp Cell Res. 2008; 314:317–329. [PubMed: 17949710]
30. Dong F, Sun X, Liu W, et al. Pitx2 promotes development of splanchnic mesoderm-derived branchiomeric muscle. Development. 2006; 133:4891–4849. [PubMed: 17107996]
31. Shih HP, Gross MK, Kioussi C. Muscle development: Forming the head and trunk muscles. Acta Histochem. 2008; 110:97–108. [PubMed: 17945333]
32. Shih HP, Gross MK, Kioussi C. Expression pattern of the homeodomain transcription factor Pitx2 during muscle development. Gene Expr Patterns. 2007; 7:441–451. [PubMed: 17166778]
33. Bendall AJ, Ding J, Hu G, et al. Msx1 antagonizes the myogenic activity of Pax3 in migrating limb muscle precursors. Development. 1999; 126:4965–4976. [PubMed: 10529415]
34. Mankoo BS, Skuntz S, Harrigan I, et al. The concerted action of Meox homeobox genes is required upstream of genetic pathways essential for the formation, patterning and differentiation of somites. Development. 2003; 130:4655–4664. [PubMed: 12925591]
35. Fukada S, Uezumi A, Ikemoto M, et al. Molecular signature of quiescent satellite cells in adult skeletal muscle. Stem Cells. 2007; 25:2448–2459. [PubMed: 17600112]
36. Watanabe S, Kondo S, Hayasaka M, et al. Functional analysis of homeodomain-containing transcription factor Lbx1 in satellite cells of mouse skeletal muscle. J Cell Sci. 2007; 120:4178–4187. [PubMed: 18003701]
37. Gross MK, Moran-Rivard L, Velasquez T, et al. Lbx1 is required for muscle precursor migration along a lateral pathway into the limb. Development. 2000; 127:413–424. [PubMed: 10603357]
38. Ono Y, Boldrin L, Knopp P, et al. Muscle satellite cells are a functionally heterogeneous population in both somite-derived and branchiomeric muscles. Dev Biol. 2010; 337:29–41. [PubMed: 19835858]
39. Brohmann H, Jagla K, Birchmeier C. The role of Lbx1 in migration of muscle precursor cells. Development. 2000; 127:437–45. [PubMed: 10603359]
40. Ochi H, Westerfield M. Lbx2 regulates formation of myofibrils. BMC Dev Biol. 2009; 9:13. [PubMed: 19216761]
41. Makarenkova HP, Gonzalez KN, Kiosses WB, et al. Barx2 controls myoblast fusion and promotes MyoD-mediated activation of the smooth muscle alpha actin gene. J Biol Chem. 2009; 284:14866–14874. [PubMed: 19269978]
42. Herring BP, Kriegel AM, Hoggatt AM. Identification of Barx2b, a serum response factor-associated homeodomain protein. J Biol Chem. 2001; 276:14482–14489. [PubMed: 11278942]
43. Meech R, Gomez M, Woolley C, et al. The homeobox transcription factor Barx2 regulates plasticity of young primary myofibers. PLoS ONE. 2010; 5:e11612. [PubMed: 20657655]
44. Edelman DB, Meech R, Jones FS. The homeodomain protein Barx2 contains activator and repressor domains and interacts with members of the CREB family. J Biol Chem. 2000; 275:21737–21745. [PubMed: 10781615]
45. Sellar GC, Li L, Watt KP, et al. BARX2 induces cadherin 6 expression and is a functional suppressor of ovarian cancer progression. Cancer Res. 2001; 61:6977–6981. [PubMed: 11585719]
46. Meech R, Makarenkova H, Edelman DB, et al. The homeodomain protein Barx2 promotes myogenic differentiation and is regulated by myogenic regulatory factors. J Biol Chem. 2003; 278:8269–8278. [PubMed: 12486129]
47. Olson LE, Zhang J, Taylor H, et al. Barx2 functions through distinct corepressor classes to regulate hair follicle remodeling. Proc Natl Acad Sci USA. 2005; 102:3708–3713. [PubMed: 15728386]

48. Makarenkova H, Becker DL, Tickle C, et al. Fibroblast growth factor 4 directs gap junction expression in the mesenchyme of the vertebrate limb bud. J Cell Biol. 1997; 138:1125–1137. [PubMed: 9281589]
49. Costes SV, Daelemans D, Cho EH, et al. Automatic and quantitative measurement of protein–protein colocalization in live cells. Biophys J. 2004; 86:3993–4003. [PubMed: 15189895]
50. Couteaux R, Mira J-C, d'Albis A. Regeneration of muscles after cardiotoxin injury. I. Cytological aspects. Biol Cell. 1988; 62:171–182. [PubMed: 3390626]
51. Rando TA, Blau HM. Primary mouse myoblast purification, characterization, and transplantation for cell-mediated gene therapy. J Cell Biol. 1994; 125:1275–1287. [PubMed: 8207057]
52. Ostle, B.; Malone, LC., editors. Statistics in Research: Basic Concepts and Techniques for Research Workers: 7. Inferences concerning two populations. 4. Iowa State University Press; Iowa 50010: 1988. p. 145-175.
53. Meech R, Edelman DB, Jones FS, et al. The homeobox transcription factor Barx2 regulates chondrogenesis during limb development. Development. 2005; 132:2135–2146. [PubMed: 15800003]
54. Zammit PS, Golding JP, Nagata Y, et al. Muscle satellite cells adopt divergent fates: A mechanism for self-renewal? J Cell Biol. 2004; 166:347–357. [PubMed: 15277541]
55. Halevy O, Piestun Y, Allouh MZ, et al. Pattern of Pax7 expression during myogenesis in the posthatch chicken establishes a model for satellite cell differentiation and renewal. Dev Dyn. 2004; 231:489–502. [PubMed: 15390217]
56. Buckingham M, Bajard L, Chang T, et al. The formation of skeletal muscle: From somite to limb. J Anat. 2003; 202:59–68. [PubMed: 12587921]
57. Bodensteiner JB, Engel AG. Intracellular calcium accumulation in Duchenne dystrophy and other myopathies: A study of 567,000 muscle fibers in 114 biopsies. Neurology. 1978; 28:439–46. [PubMed: 76996]
58. Garry DJ, Meeson A, Elterman J, et al. Myogenic stem cell function is impaired in mice lacking the forkhead/winged helix protein MNF. Proc Natl Acad Sci. 2000; 97:5416–5421. [PubMed: 10792059]
59. Hashimoto N, Murase T, Kondo S, et al. Muscle reconstitution by muscle satellite cell descendants with stem cell-like properties. Development. 2004; 131:5481–5490. [PubMed: 15469979]
60. Lancioni H, Lucentini L, Palomba A, et al. Muscle actin isoforms are differentially expressed in human satellite cells isolated from donors of different ages. Cell Biol Int. 2007; 31:180–185. [PubMed: 17137797]
61. Stevens TA, Meech R. BARX2 and estrogen receptor-*a* (ESR1) coordinately regulate the production of alternatively spliced ESR1 isoforms and control breast cancer cell growth and invasion. Oncogene. 2006; 25:5426–5435. [PubMed: 16636675]
62. Stern-Straeter J, Bran G, Riedel F, et al. Characterization of human myoblast cultures for tissue engineering. Int J Mol Med. 2008; 21:49–56. [PubMed: 18097615]
63. Siegel AL, Atchison K, Fisher KE, et al. 3D timelapse analysis of muscle satellite cell motility. Stem Cells. 2009; 27:2527–2538. [PubMed: 19609936]
64. Sicinski P, Geng Y, Ryder-Cook AS, et al. The molecular basis of muscular dystrophy in the mdx mouse: A point mutation. Science. 1989; 244:1578–1580. [PubMed: 2662404]
65. Anderson JE, Ovalle WK, Bressler BH. Electron microscopic and autoradiographic characterization of hindlimb muscle regeneration in the mdx mouse. Anat Rec. 1987; 219:243–257. [PubMed: 3425943]
66. Carnwath JW, Shotton DM. Muscular dystrophy in the mdx mouse: histopathology of the soleus and extensor digitorum longus muscles. J Neurol Sci. 1987; 80:39–54. [PubMed: 3612180]
67. Coulton GR, Morgan JE, Partridge TA, et al. The mdx mouse skeletal muscle myopathy. I. A histological, morphometric and biochemical investigation. Neuropathol Appl Neurobiol. 1988; 14:53–70. [PubMed: 2967442]
68. Chamberlain JS, Metzger J, Reyes M, et al. Dystrophin-deficient mdx mice display a reduced life span and are susceptible to spontaneous rhabdomyosarcoma. FASEB J. 2007; 21:2195–2204. [PubMed: 17360850]

69. Inanlou MR, Dhillon GS, Belliveau AC, et al. A significant reduction of the diaphragm in mdx:MyoD$^{-/-}$ (9th) embryos suggests a role for MyoD in the diaphragm development. Dev Biol. 2003; 261:324–336. [PubMed: 14499644]
70. Ferrari G, Cusella-De Angelis G, Coletta M, et al. Muscle Regeneration by bone marrow-derived myogenic progenitors. Science. 1998; 279:1528–1530. [PubMed: 9488650]
71. Gussoni E, Soneoka Y, Strickland CD, et al. Dystrophin expression in the mdx mouse restored by stem cell transplantation. Nature. 1999; 401:390–394. [PubMed: 10517639]
72. Polesskaya A, Seale P, Rudnicki MA. Wnt signaling induces the myogenic specification of resident CD45+ adult stem cells during muscle regeneration. Cell. 2003; 113:841–852. [PubMed: 12837243]
73. Mitchell KJ, Pannérec A, Cadot B, et al. Identification and characterization of a non-satellite cell muscle resident progenitor during postnatal development. Nat Cell Biol. 2010; 12:257–266. [PubMed: 20118923]
74. Mansouri A, Stoykava A, Torres M, et al. Dysgenesis of cephalic neural crest derivatives in Pax7$^{-/-}$ mutant mice. Development. 1996; 122:831–838. [PubMed: 8631261]
75. Olguin HC, Olwin BB. Pax-7 up-regulation inhibits myogenesis and cell cycle progression in satellite cells: A potential mechanism for self-renewal. Dev Biol. 2004; 275:375–88. [PubMed: 15501225]
76. Lepper C, Conway SJ, Fan C-M. Adult satellite cells and embryonic muscle progenitors have distinct genetic requirements. Nature. 2009; 460:627–631. [PubMed: 19554048]
77. Mege RM, Goudou D, Diaz C, et al. N-cadherin and N-CAM in myoblast fusion: Compared localisation and effect of blockade by peptides and antibodies. J Cell Sci. 1992; 103:897–906. [PubMed: 1487503]
78. Peck D, Walsh FS. Differential effects of over-expressed neural cell adhesion molecule isoforms on myoblast fusion. J Cell Biol. 1993; 123:1587–1595. [PubMed: 8253853]
79. Zeschnigk M, Kozian D, Kuch C, et al. Involvement of M-cadherin in terminal differentiation of skeletal muscle cells. J Cell Sci. 1995; 108:2973–2981. [PubMed: 8537437]
80. Irintchev A, Zeschnigk M, Starzinski-Powitz A, et al. Expression pattern of M-cadherin in normal, denervated, and regenerating mouse muscles. Dev Dyn. 1994; 199:326–337. [PubMed: 8075434]
81. Wróbel E, Brzóska E, Moraczewski J. M-cadherin and β-catenin participate in differentiation of rat satellite cells. Eur J Cell Biol. 2007; 86:99–109. [PubMed: 17222478]
82. Dangott B, Schultz E, Mozdziak PE. Dietary creatine monohydrate supplementation increases satellite cell mitotic activity during compensatory hypertrophy. Int J Sports Med. 2000; 21:13–16. [PubMed: 10683092]
83. Schultz E, Jaryszak DL, Valliere CR. Response of satellite cells to focal skeletal muscle injury. Muscle Nerve. 1985; 8:217–222. [PubMed: 4058466]
84. Furling D, et al. Defective satellite cells in congenital myotonic dystrophy. Human Mol Genet. 2001; 10:2079–2087. [PubMed: 11590125]
85. Lefaucheur JP, Pastoret C, Sebille A. Phenotype of dystrophinopathy in old mdx mice. Anat Rec. 1995; 242:70–76. [PubMed: 7604983]
86. Parker AE, Robb SA, Chambers J, et al. Analysis of an adult Duchenne muscular dystrophy population. QJM. 2005; 98:729–736. [PubMed: 16135534]

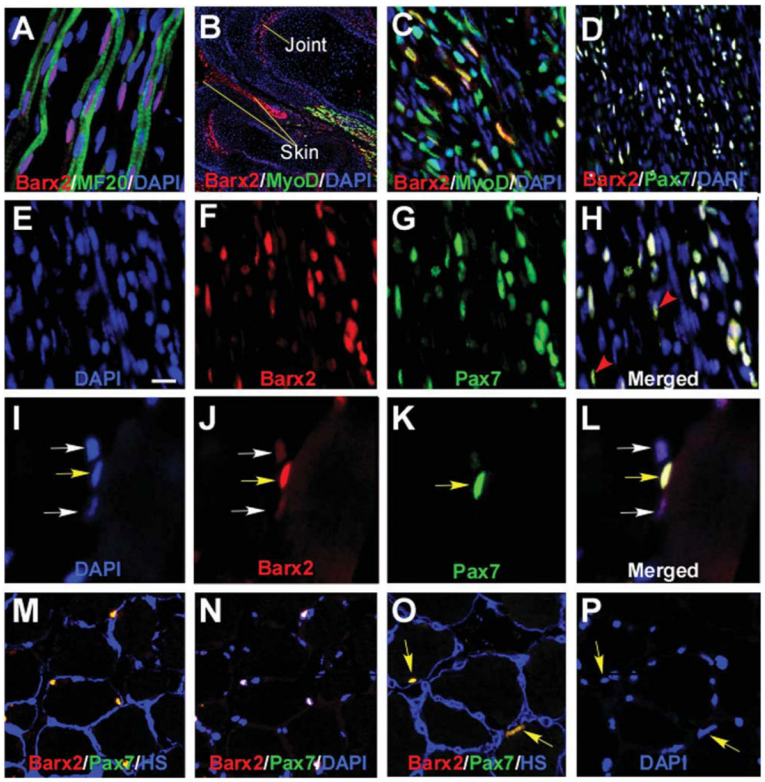

Figure 1.

Barx2 is expressed in embryonic and adult muscle. **(A–C):** E13.5 limb muscle. (A): Barx2 (red) is expressed in primary myofibers marked with the MF20 antibody (green) as well as between fibers. DAPI, blue. (B, C): Barx2 (red) and MyoD (green) coexpression is shown in a subset of muscle nuclei in the distal hind limb of E13.5 embryo. The image in (B) shows two adjacent digits, and Barx2 expression is also seen in skin and presumptive joint region (arrows). (C):Higher magnification of the muscle shown in (B). **(D–H):** E18 limb muscle; Barx2 expression overlaps extensively with Pax7 (Barx2, red; Pax7, green; DAPI, blue). Red arrowheads indicate Pax7-positive nuclei with low level of Barx2 expression. **(I–P):** Adult muscle; (I–L): Yellow arrows indicate nuclei in which Barx2 and Pax7 are coexpressed; White arrows indicate nuclei with weaker expression of Barx2 and no apparent expression of Pax7. **(M–P):** Barx2 is coexpressed with Pax7 in nuclei situated under the basal lamina. (M, O): Overlap of Barx2 (red) and Pax7 (green) staining is seen as yellow; the basal lamina is labeled with antibody to HS, blue. (N): The same section shown in (M) but labeled with Barx2 (red), Pax7 (green) and DAPI (blue), and without HS staining; nuclei that colocalize DAPI, Barx2, and Pax7 are white. (P): The same section shown in (O) but labeled with DAPI only (blue). Yellow arrows in (O) and (P) show nuclei expressing both Barx2 and Pax7 in (O). Abbreviations: DAPI, 4′,6-diamidino-2-phenylindole; HS, heparan sulfate.

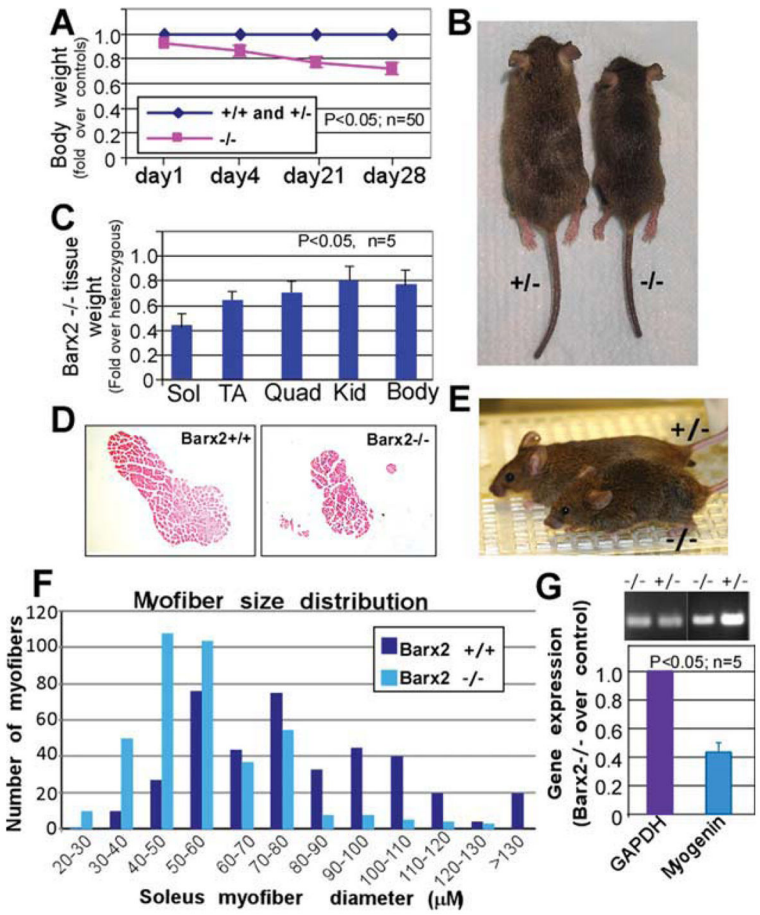

Figure 2.

Analysis of postnatal muscle growth in *Barx2* mutant mice. **(A):** Between 1 and 28 days, *Barx2*$^{-/-}$ pups show significant reduction in growth as indicated by total body weight relative to *Barx2*$^{+/+}$ and *Barx2*$^{+/-}$ littermates. The averaged weights of the wild-type and heterozygous mice were taken as the baseline. The statistical difference was observed at $p < .05$, *n*, number of mice per genotype. **(B):** Typical appearance of *Barx2*$^{+/-}$ and *Barx2*$^{-/-}$ mice at 28 days (wild-type and heterozygous mice are indistinguishable). (**C):** Sol, TA, and Quad muscles from four pairs of 4-week old *Barx2*$^{-/-}$ and *Barx2*$^{+/-}$ littermates were harvested and weighed (*n*, number of mice). (**D):** Transverse sections of Sol muscle from wild-type and *Barx2*$^{-/-}$ *mice* were stained with hematoxylin and eosin. **(E):** Example of a 16-month-old Barx2 null mouse displaying a hunched back and splayed stance relative to a heterozygous control mouse. **(F):** Histogram demonstrating the distribution of myofiber sizes in *Barx2*$^{-/-}$ and *Barx2*$^{+/+}$ mice. Maximal myofiber diameters were measured in transverse sections of Sol muscle from three mice for each genotype; number of myofibers. $n = 396$ for *Barx2*$^{+/+}$ and 392 for *Barx2*$^{-/-}$. **(G):** Expression of the muscle differentiation marker myogenin is reduced in muscles from 4-week-old *Barx2*$^{-/-}$ mice relative to *Barx2*$^{+/-}$ littermates as indicated by semiquantitative RT-PCR (*n*, number of mice). GAPDH is used as a reference standard. Abbreviations: GAPDH, glyceraldehyde-3-phosphate

dehydrogenase; Kid, kidney; Quad, quadriceps; RT-PCR, reverse transcriptase polymerase chain reaction; Sol, Soleus; TA, tibialis anterior.

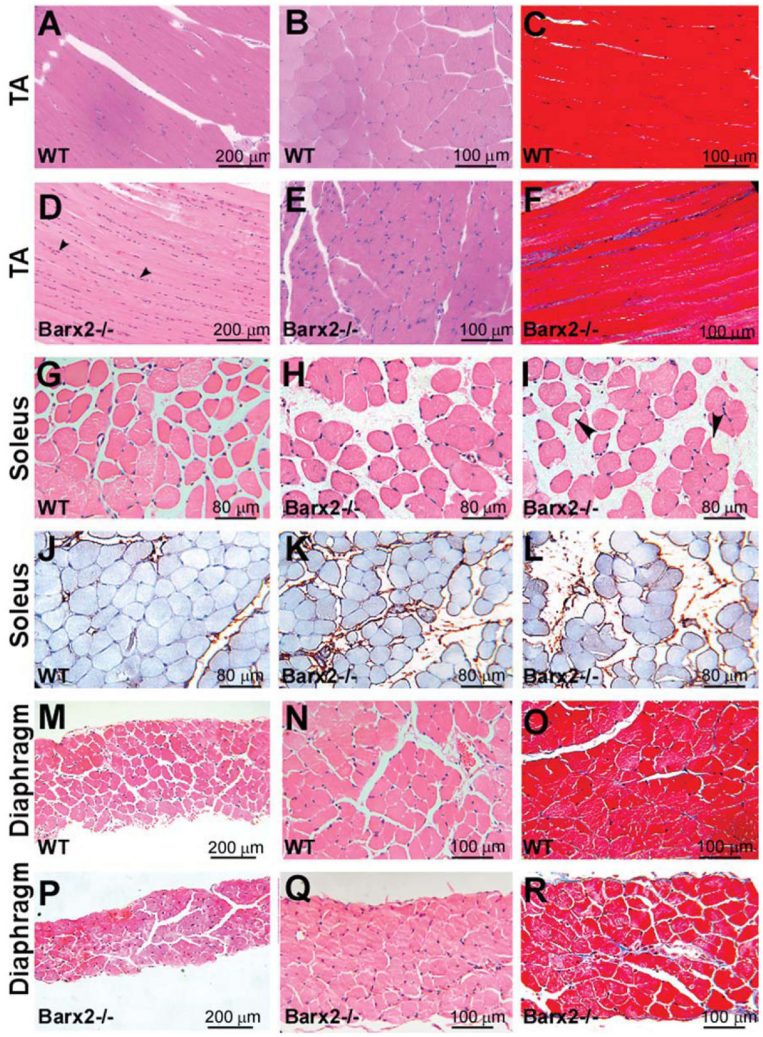

Figure 3.

Histological analysis of muscle in adult *Barx2* mutant mice. **(A–F):** Comparison of TA muscle in 6-month-old WT (A–C) and *Barx2*−/− mice (D–F). Relative to wild-type muscle, *Barx2*$^{-/-}$ muscle shows narrower myofibers, an increased number of nuclei between myofibers, and increased fibrosis, as indicated by Masson's trichrome staining (panels C and F). **(G–L):** Comparison of soleus muscle in 6-month-old wild-type (G) and *Barx2*$^{-/-}$ (H, I) mice. Relative to wild-type muscle, *Barx2*$^{-/-}$ muscle exhibits a larger distance between myofibers and increased collagen deposition between myofibers (as shown by collagen I immunostaining in J–L). Myofibers in *Barx2*$^{-/-}$ muscle were generally more rounded, although some showed an angulated morphology with cytoplasmic vacuoles (I, black arrowheads). **(M–R):** Comparison of diaphragm in 6-month-old wild-type (M–O) and *Barx2*$^{-/-}$ (P–R) mice. The diaphragm of *Barx2*$^{-/-}$ mice is much thinner than that of wild-type mice and moderately fibrotic as indicated by Masson's trichrome staining (panels O and R). A, B, D, E, G, H, M, N, P, and Q, hematoxylin and eosin staining; (J–L), collagen I immunostaining (brown) with iron hematoxylin counterstain; C, F, O, and R, Masson's trichrome staining. Abbreviations: TA, tibialis anterior; WT, wild type.

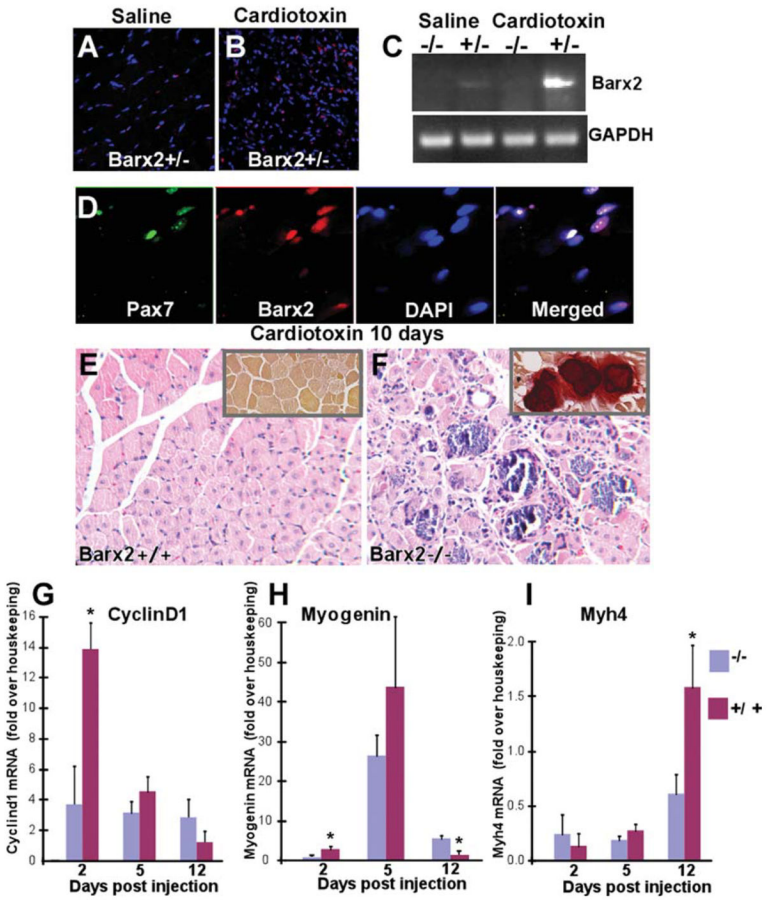

Figure 4.

Barx2 is important for muscle regeneration. **(A, B):** Regenerating cardiotoxin (CTX)-injected muscle (B) shows a dramatic increase in Barx2-expressing nuclei (red) when compared to saline-injected muscle (A). **(C):** RT-PCR shows that Barx2 expression is upregulated in regenerating CTX-injected muscle relative to saline-injected muscle. A representative result is shown; similar upregulation was seen in replicate experiments. **(D)**: Barx2-expressing cells also express Pax7 (green). **(E):** Hematoxylin-eosin-stained paraffin sections of *Barx2*$^{+/-}$ TA muscles harvested 10 days after CTX injection show efficient muscle regeneration indicated by centrally located nuclei in almost all myotubes. **(F):** In contrast, sections of *Barx2*$^{-/-}$ muscle harvested 10 days after injection show disorganized morphology with necrotic fibers, myotubes of different sizes, and undifferentiated myoblasts. Alizarin red staining also reveals calcium deposits in *Barx2*$^{-/-}$ muscle (insets). **(G, H, I):** Quantitative RT-PCR analysis of cyclin-D1 (G), myogenin (H), and myosin heavy chain (I) expression at 2, 5, and 12 days after CTX injection in the TA muscle. Gene expression data from the cardiotoxin-treated limb was normalized to that from the saline (vehicle)-treated contralateral limb and to a pool of housekeeping genes. Three mice of each genotype were used per time point. Abbreviations: DAPI, 4′,6-diamidino-2-phenylindole; GAPDH, glyceraldehyde-3-phosphate dehydrogenase; RT-PCR, reverse transcriptase polymerase chain reaction; TA, tibialis anterior.

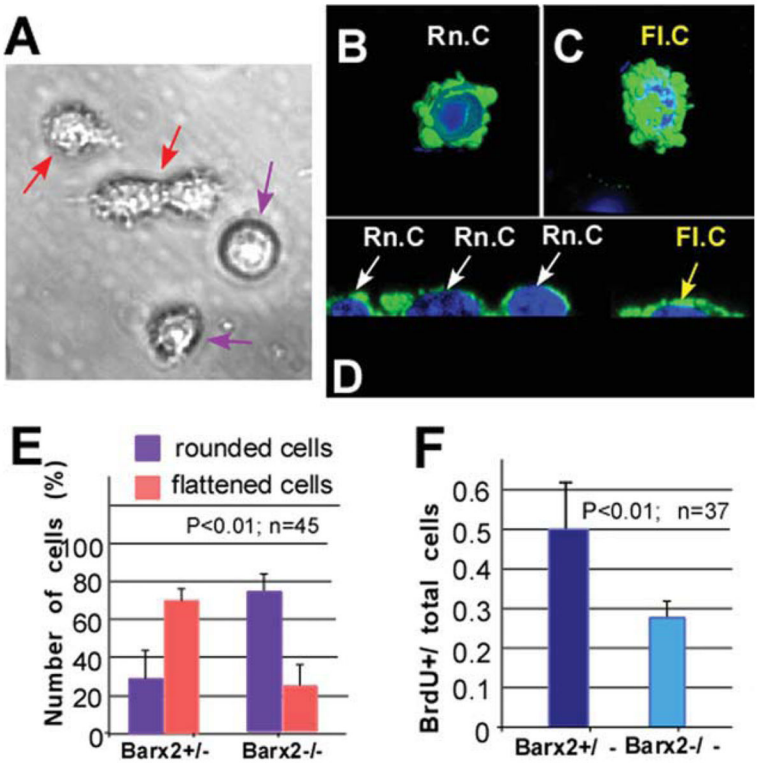

Figure 5.

Primary myoblast cultures from *Barx2*$^{-/-}$ muscle show altered morphology and reduced proliferation. **(A):** Myoblast cultures maintained in growth media contain a mixture of two types of cells: relatively rounded cells with smooth membranes (violet arrows) and slightly elongated cells with more processes (red arrows). **(B–D):** Confocal microscopy and serial 3D reconstruction performed using IMARIS software show that these two populations correspond to rounded (Rn.c; white arrows) (B, D) or elongated/flattened cells (Fl.c; yellow arrows) as is most apparent in transverse optical sections (C, D). Green, smooth muscle actin antibody staining; blue, DAPI. **(E):** Cells displaying rounded or flattened morphologies were counted in confocal microscopy images, revealing that cells with the flattened morphology predominate in *Barx2*$^{+/-}$ cultures, whereas cells with rounded morphology predominate in *Barx2*$^{-/-}$ cultures. **(F):** Reduced proliferation in *Barx2*$^{-/-}$ cultures relative to *Barx2*$^{+/-}$ cultures as measured by BrdU incorporation. In panels (E) and (F), *n* indicates number of fields per genotype used for quantification. Replicate experiments with independent myoblast isolates gave similar results. Abbreviation: BrdU, Bromodeoxyuridine.

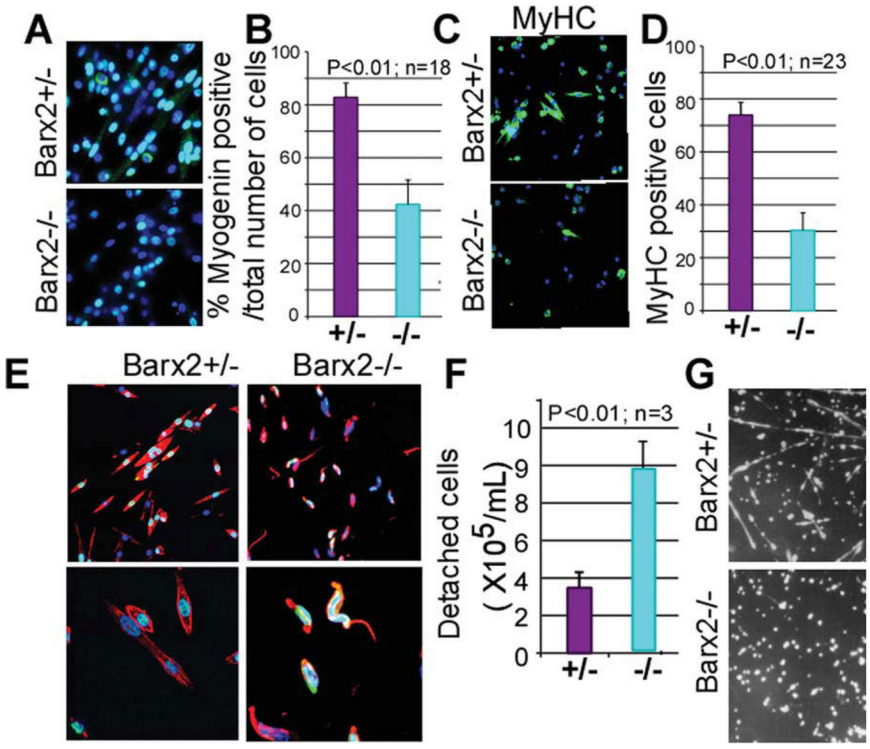

Figure 6.

Primary myoblasts from *Barx2*$^{-/-}$ muscle have poor adhesion and show delayed differentiation. **(A–D):** Differentiation was induced in myoblast cultures by serum withdrawal, and gene expression was examined after 6 (A, B) and 24 (C, D) hours. At 6 hours after serum withdrawal, *Barx2*$^{-/-}$ cultures show almost twofold reduction in the number of myogenin-expressing cells relative to *Barx2*$^{+/-}$ cultures suggesting a delay in the onset of differentiation (A, B); green, myogenin; blue, DAPI. At 24 hours after serum withdrawal, *Barx2*$^{-/-}$ cultures show fewer myotubes and reduced expression of MyHC relative to *Barx2*$^{+/-}$ cultures (C, D); green, MyHC; blue, DAPI. In panels (B) and (D), *n* indicates number of fields per genotype used for quantification. Replicate experiments with independent myoblast isolates gave similar results. **(E):** At 72 hours after serum withdrawal, myotubes in *Barx2*$^{-/-}$ cultures begin to detach from the plate. Red, F-actin, blue, DAPI. **(F):** *Barx2*$^{-/-}$ cells plated on fibronectin detach more readily than *Barx2*$^{+/-}$ cells in a plate-washing assay (*n*, number of independent experiments). **(G):** *Barx2*$^{+/-}$ myoblasts plated on fibronectin form myotubes in approximately 72 hours whereas *Barx2*$^{-/-}$ myoblasts do not. Abbreviations: DAPI, 4′,6-diamidino-2-phenylindole; MyHC, myosin heavy chain.

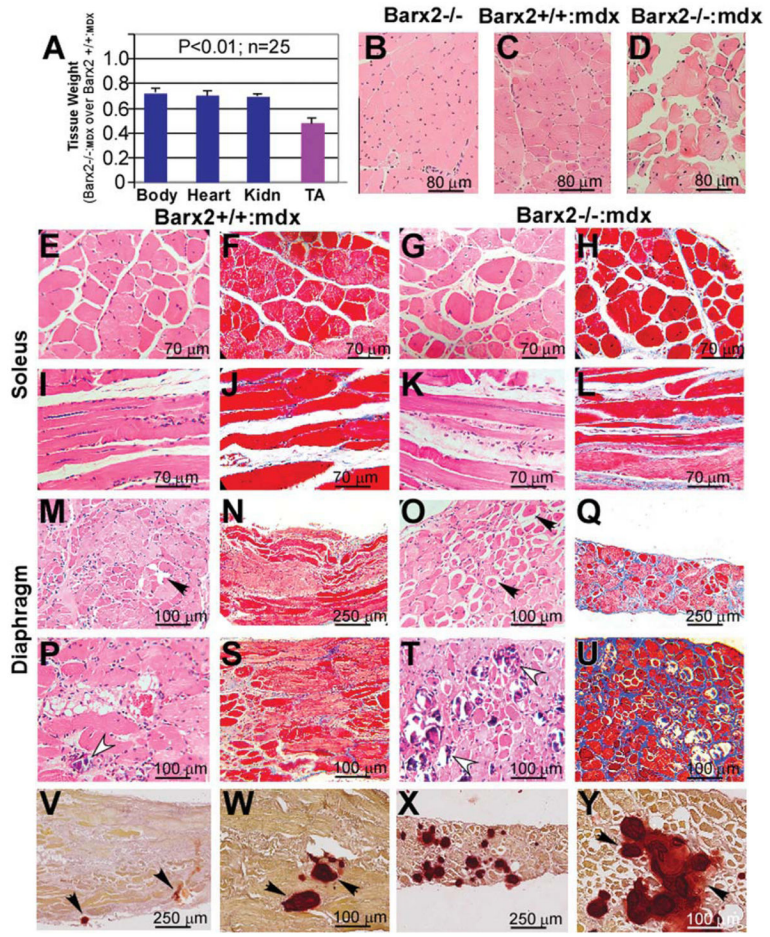

Figure 7.

Phenotype of *Barx2/mdx* double null mice. **(A):** Comparison of total body, heart, Kidn, and TA weights in *Barx2*$^{-/-}$*:mdx* (shown as a ratio of *Barx2*$^{-/-}$*:mdx* over *Barx2*$^{+/+}$*:mdx* weights). TA muscle shows a dramatic reduction in weight relative to other organs. Tissues were harvested and weighed from 4-week-old *Barx2*$^{+/+}$*:mdx* and *Barx2*$^{-/-}$*:mdx* sibling pairs (*n*, number of pairs studied). **(B–D):** Hematoxylin-eosin (H&E)-stained paraffin sections of TA muscles obtained from 6-month-old *Barx2*$^{-/-}$, *Barx2*$^{+/+}$*:mdx*, and *Barx2*$^{-/-}$*:mdx* mice. Double knockout TA muscle shows variability of fiber size suggesting presence of atrophy and hypertrophy of myofibers (D). **(E–L):** Soleus muscle of *Barx2*$^{-/-}$*:mdx* mice (G, K, H&E staining; H, L, trichrome staining) shows greater variability in myofiber size and shape and marked endomysial and perimysial fibrosis relative to soleus muscle of *Barx2*$^{+/+}$*:mdx* mice (E, I, H&E staining; F, J, trichrome staining). **(M–U):** Diaphragm muscles of 6-month-old (M–Q) and 12-month-old (P–U) *Barx2*$^{+/+}$*:mdx* (M, P, H&E staining; N, S, trichrome staining) and *Barx2*$^{-/-}$*:mdx* (O, T, H&E staining; Q, U, trichrome staining) mice. Diaphragms of 6-month-old *Barx*$^{-/-}$*:mdx* mice appear much thinner than diaphragms of *Barx2*$^{+/+}$*:mdx* mice (compare N and Q). In addition, diaphragms of 6-month-old *Barx2*$^{-/-}$*:mdx* mice show frequent rounded atrophic fibers (black arrows). Atrophic fibers are dark red and glassy (they represent hypercontracted fibers). Trichrome staining shows more extensive fibrosis in six *Barx2*$^{-/-}$*:mdx* diaphragms relative to *Barx2*$^{+/+}$*:mdx*

diaphragms (compare N and Q). The diaphragms of 12-month-old *Barx2*$^{-/-}$*:mdx* mice show extensive fibrosis and greater instance of focal myofiber fibrosis (compare S and U), and necrotic myofibers undergoing myophagocytosis (T, white arrowheads) relative to *Barx2*$^{+/+}$*:mdx* mice (P, white arrowhead). **(V–Y):** Alizarin red staining reveals increased calcium deposits in the *Barx2−/−:mdx* diaphragm muscle (X, Y) relative to *Barx2*$^{+/+}$*:mdx* muscle (V, W). Abbreviations: Kidn, kidney; TA, tibialis anterior.